JACS
JOURNAL OF THE AMERICAN CHEMICAL SOCIETY
Article
Cite This: J. Am. Chem. Soc. 2019, 141, 16046−16056
pubs.acs.org/JACS

Mechanism and Origins of Enantioselectivities in Spirobiindane-Based Hypervalent Iodine(III)-Induced Asymmetric Dearomatizing Spirolactonizations

Hanliang Zheng,[†] Yueqian Sang,[†] K. N. Houk,*[,‡] Xiao-Song Xue,*[,†] and Jin-Pei Cheng[†]

[†]State Key Laboratory of Elemento-Organic Chemistry, College of Chemistry, Nankai University, Tianjin 300071, People's Republic of China

[‡]Department of Chemistry and Biochemistry, University of California, Los Angeles, California 90095, United States

Supporting Information

ABSTRACT: The work of Kita et al. on asymmetric oxidative dearomatization of naphthol carboxylic acids to spirolactones mediated/catalyzed by a novel, conformationally rigid μ-oxo-bridged hypervalent iodine(III) species is a landmark discovery in enantioselective iodine(III) catalysis [Kita, Y.; et al. *Angew. Chem., Int. Ed.* **2008**, *47*, 3787. DOI: 10.1002/anie.200800464; *J. Am. Chem. Soc.* **2013**, *135*, 4558. DOI: 10.1021/ja401074u]. We have investigated the detailed mechanism of this important transformation using density functional theory. Calculations revealed that proton transfer from the pendant carboxylic acid of naphthols to the bridging oxygen atom or the ligand of iodine(III) species, which enhances the nucleophilicity of the carboxylic oxygen and the nucleofugality of the iodoarene, is crucial for the dearomatizing spirolactonization. Halogen bonding between the resulting carboxylate and the electron-deficient iodine(III) center further stabilizes the dearomatizing spirolactonization transition states. Calculations also revealed a long-neglected cleaved μ-oxo iodine(III) species that is more reactive but less selective than the μ-oxo-bridged hypervalent iodine(III) species itself for the oxidative dearomatization of naphthols. The coexistence of two sequential dearomatizing spirolactonization processes in the reaction system results in a lower enantioselectivity. A new stereochemical model that is able to reproduce and rationalize the observed apparent enantioselectivities is proposed.

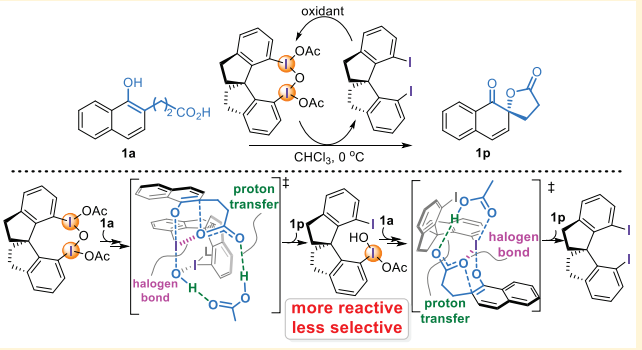

INTRODUCTION

Hypervalent iodine reagents are intensively used in organic chemistry as a safe, mild, and economical alternative to heavy metal or rare metal reagents.[1] Their unique reactivities inspire the exploration of new synthetic transformations that would be difficult to accomplish otherwise.[1] Recently, special attention has focused on asymmetric transformations induced by chiral hypervalent iodine reagents or catalysts.[2] Notable asymmetric reactions developed include α-functionalization of ketones,[3] difunctionalization of alkenes,[4] oxidative dearomatization of phenols,[5] and many others.[2] However, stereochemical models[6] and mechanistic discussions[7] of these transformations are still in their infancy.

Dearomatization of phenols is a powerful strategy for the synthesis of complex molecules, providing an avenue for simultaneously introducing stereochemical information and generating products that are primed for further reaction.[8] The main challenge in making them asymmetric is to control the reaction selectivity while overcoming the loss of aromaticity.[8c] This is particularly true for hypervalent iodine-mediated/catalyzed oxidative dearomatization. The development of chiral hypervalent iodines as stoichiometric reagents or catalysts with high efficiency and satisfactory enantioselectivity has long been a challenging task.[5]

A breakthrough was achieved in 2008 when Kita and co-workers disclosed a novel conformationally rigid, μ-oxo-bridged iodine(III) reagent **R1** based on the axially chiral spirobiindane scaffold (Scheme 1a).[5a] With this reagent, they established the first protocol for enantioselective oxidative dearomatization of naphthol carboxylic acids at an unprecedented level of asymmetric induction in the field of hypervalent iodine-mediated transformations. Intriguingly, the use of other chiral iodoarenes **R3** and **R4** resulted in formation of almost racemic spirolactones (Scheme 1a). They also demonstrated that spirobiindane **C1** could be used in catalytic quantities, along with *meta*-chloroperbenzoic acid (*m*CPBA) as a stoichiometric oxidant, with some diminution in enantioselectivity (up to 69% ee) (Scheme 1b). The enantioselectivity can be enhanced through the introduction of ethyl-substituents at the *ortho*-positions of the iodine atoms (Scheme 1b).[5c] Kita proposed a transition state (TS) model to rationalize the

Received: July 31, 2019
Published: September 13, 2019

DOI: 10.1021/jacs.9b08243
J. Am. Chem. Soc. 2019, 141, 16046−16056

Scheme 1. Asymmetric Kita Spirolactonization

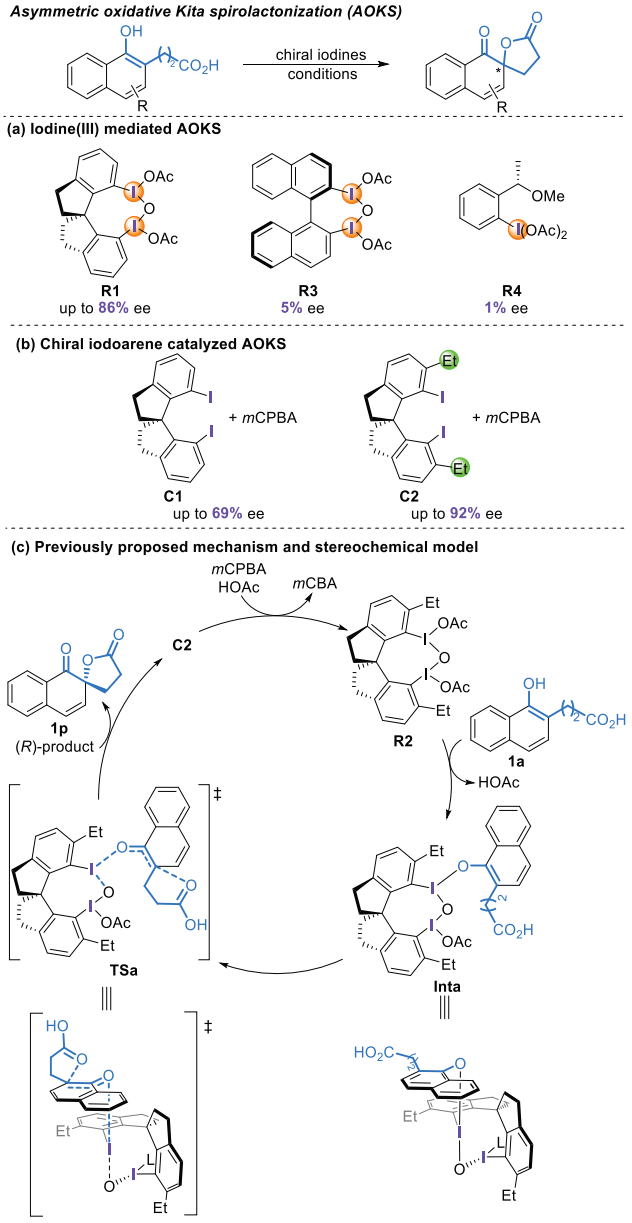

observed stereoselectivities (Scheme 1c). In this model, the *in situ*-generated iodine(III) catalyst **R2** undergoes a ligand exchange with the naphthol oxygen to provide the intermediate **Inta**, and then the pendant carboxylic acid preferentially attacks at the *ipso* position of the naphthol ring from the less hindered *Re*-face, yielding the observed *R* enantiomer of the product. This discovery has been regarded as a landmark in enantioselective iodine(III) catalysis, proving the chiral iodine compound as a new entrance to asymmetric organocatalysis.

We have studied computationally the mechanism and origins of stereoselectivities of the asymmetric oxidative dearomatization of naphthol carboxylic acids involving the μ-oxo-bridged hypervalent iodine(III) species. A revised mechanism and stereochemical model are proposed. The new stereochemical model is highly consistent with the observed experimental stereoselectivities and sheds light on the advantage of rigid versus flexible catalysts.[9]

COMPUTATIONAL METHODS

Quantum chemical calculations were carried out with the Gaussian 09 package.[10] The hybrid-meta GGA functional M06-2X[11] with a mixed basis set of SDD[12] for I and 6-31G(d) for other atoms was employed for optimizing the geometries of minima and transition states. The SMD[13] implicit solvation model was used to account for solvation effects of chloroform or dichloromethane. Frequency calculations were performed at the same level to verify the nature of stationary points. Previous computational studies of hypervalent iodine compounds-mediated reactions with the M06-2X functional provided results in accord with experiment.[6c,7e,14] To obtain more accurate energies, single point energy calculations were performed at the SMD-M06-2X/cc-pVTZ(-PP)[15] level of theory. Gibbs free energies are corrected using Truhlar et al.'s quasi-harmonic approximation by setting all positive frequencies that are less than 100 cm^{-1} to 100 cm^{-1}.[16] Non-covalent interaction analysis was performed by NCIPLOT.[17] The structures were generated by CYLview[18] and Pymol.[19] All energies reported throughout the text are in kcal mol^{-1}, and the bond lengths are in angstroms (Å).

RESULTS AND DISCUSSION

Mechanism of the Spirobiindane-Based μ-Oxo-Bridged Hypervalent Iodine(III)-Induced Asymmetric Dearomatizing Spirolactonization. The spirobiindane-based iodine(III) reagent **R1**-promoted asymmetric dearomatizing spirolactonization of propanoic acid-substituted 1-naphthol **1a** (Scheme 2) was chosen as the model reaction

Scheme 2. Model Reaction Chosen for Calculation

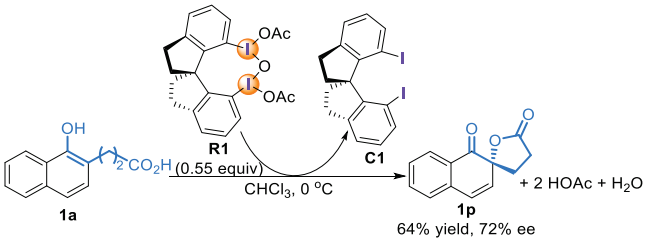

for investigating the mechanistic details. We began our study by exploring the ligand exchange/direct spirolactonization mechanism proposed by Kita (Scheme 1c). The computed reaction coordinate diagrams are given in Figure 1 and Figure S1. Optimized geometries of some key transition structures and intermediates are presented in Figure 2. Although the ligand exchange is viable with a barrier of 18.8 kcal mol^{-1} via **TS1a**, a direct attack of the *ipso* position of the naphthol ring by the pendant carboxylic acid via **TS2a-(*R*)** to furnish the spirolactonization product has an activation free energy barrier as high as 48.2 kcal mol^{-1} (see Figure S1). The direct spirolactonization mechanism is thus unlikely to account for these reactions.

We located a hydrogen-bond-assisted ligand-exchange transition state **TS1b** (Figure 1a), which is 0.5 kcal mol^{-1} more stable than the non-hydrogen-bond-assisted ligand-exchange transition state **TS1a** (Figure S1). The resulting **Int1b** undergoes proton transfer to generate **Int2b**, which is located 10.1 kcal mol^{-1} above **Int1b**. The barrier for the subsequent dearomatizing spirolactonization through **TS2b-(*R*)** is 28.9 kcal mol^{-1} (Figure 1a), which is 19.3 kcal mol^{-1} lower than that of the direct spirolactonization via **TS2a-(*R*)** (Figure S1). However, this activation free energy barrier, 28.9 kcal mol^{-1}, is considered to be still too high, given the fact that these reactions can occur readily at 0 °C.

DOI: 10.1021/jacs.9b08243
J. Am. Chem. Soc. 2019, 141, 16046−16056

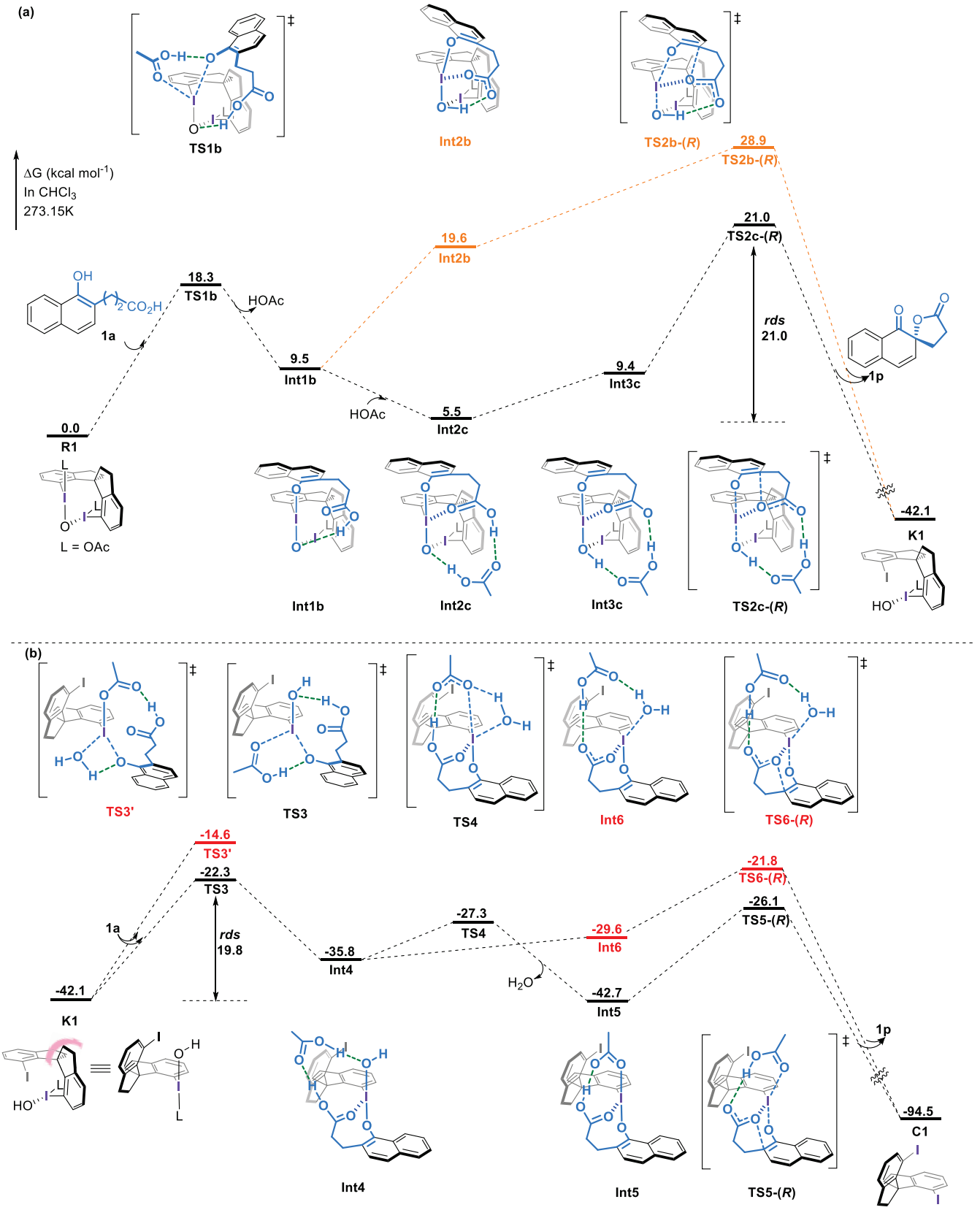

Figure 1. Calculated potential energy profile (kcal mol^{-1}) for (a) the μ-oxo-bridged hypervalent iodine(III) species **R1** and (b) the *in situ*-formed iodine(III) species **K1**-mediated asymmetric oxidative Kita spirolactonization.

Inspired by Wheeler's study.[20] and Yu's proton shift theories,[21] we explored whether the barrier could be further reduced by recruiting an acetic acid molecule as a hydrogen-bonding bridge between the carboxylic acid group in **1a** and the bridging oxygen atom in **R1**. Indeed, the inclusion of an acetic acid lowers the energies of the intermediates and

DOI: 10.1021/jacs.9b08243
J. Am. Chem. Soc. 2019, 141, 16046−16056

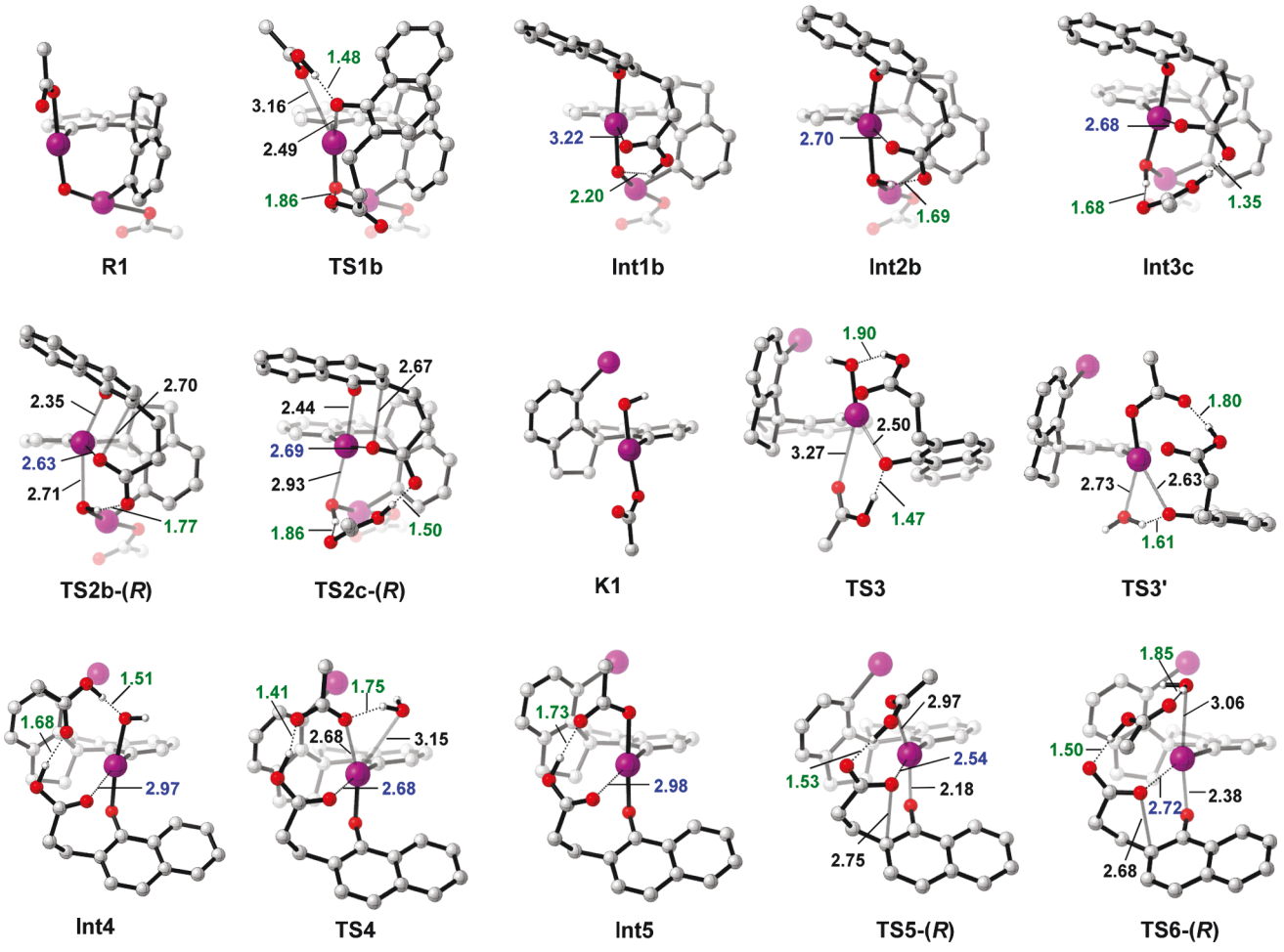

Figure 2. Calculated geometries of transition structures and intermediates for the μ-oxo-bridged hypervalent iodine(III) species **R1**-mediated asymmetric oxidative Kita spirolactonization.

transition states (Figure 1a). The overall activation free energy barrier proceeding via **TS2c-(*R*)** is now reduced to 21.0 kcal mol^{-1}, likely as a result of the strain release induced by the formation of an acetic acid hydrogen bonding bridge. The breaking O---I(III)---O 3-center-4-electron (3c-4e) bond[1b] in **TS2c-(*R*)** is close to 180° but deviated significantly from 180° in **TS2b-(*R*)** (Figure 3), indicating a smaller angle strain in the former TS structure. Previous computational and experimental studies have shown that hypervalent iodine compounds can act as a nonclassical halogen bond donor.[1b,6c,22] A closer examination of the structures of **Int2c** and **TS2c-(*R*)** reveals O---I(III) distances are considerably shorter than the sum of the van der Waals radii (Figure 2). This suggests nonclassical halogen bonding interactions[1b,23] between the carboxylic oxygen and the electron-deficient iodine(III) center (Figure 4), which further stabilize these structures.

Formation of the phenoxenium ion through a dissociative mechanism has been generally proposed for iodine(III)-mediated oxidative dearomatization of phenols. Our calculations show that the dissociation transition state **TS2c-Dis** that leads to the phenoxenium ion intermediate, is 5.2 kcal mol^{-1} higher in free energy than the spirolactonization transition state **TS2c-(*R*)** (Figure S2). This indicates that the dissociative pathway is unable to compete with the spirolactonization process for this reaction. However, when a strong electron-donating substituent presents on the naphthol ring of substrate, the dissociative pathway might be able to compete with the spirolactonization process.

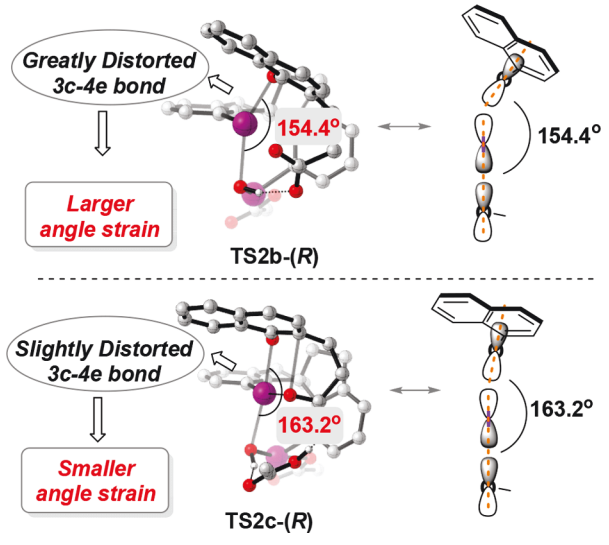

Figure 3. Angle of the breaking O---I(III)---O 3-center-4-electron bond in **TS2b-(*R*)** and in **TS2c-(*R*)**.

Generation of the spirolactonization product **1p** and the cleaved μ-oxo iodine(III) species **K1** (a half-reduced form of the μ-oxo-bridged hypervalent) is highly exergonic by 42.1 kcal

DOI: 10.1021/jacs.9b08243
J. Am. Chem. Soc. 2019, 141, 16046−16056

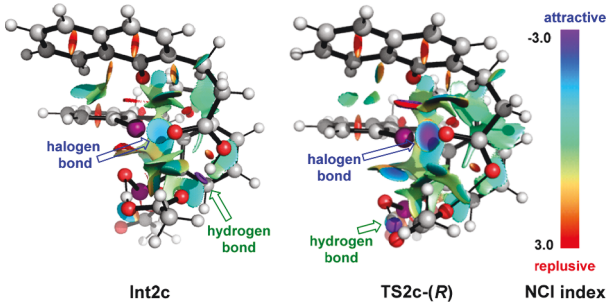

Figure 4. Non-covalent interactions analysis for **Int2c** and **TS2c-(*R*)** structures. (blue, strongly attractive; green, weakly attractive; red, strongly repulsive).

mol^{-1}. Notably, the iodine(III) center in **K1** may also serve as an active center to promote dearomatizing spirolactonization. In fact, in the original studies of Kita, 0.55 equiv **R1** was found to be efficient for conversion of one equiv of substrate, and the iodoarene was recovered after reactions (Scheme 2).[5a] The second iodine(III) center is required to participate in the dearomatizing spirolactonization. Accordingly, we also investigated the mechanism of **K1**-mediated spirolactonization. The results are presented in Figure 1b.

In principle, both OH and OAc in **K1** could undergo ligand exchange with the naphthol oxygen of **1a**. As shown in Figure 1b, ligand exchange with OAc (**TS3**) is 7.7 kcal mol^{-1} more favored than with OH (**TS3′**), consistent with previous observation that the OH ligand has a stronger *trans* influence that weakens the *trans* I-OAc bond.[24] In analogy to intermediate **Int1b,** the resulting **Int4** could undergo proton transfer and spirolactonization to provide another molecule of product. The barrier for dearomatizing spirolactonization via **TS6-(*R*)** is 14 kcal mol^{-1} with respect to **Int4**. Alternatively, we found that **Int4** could undergo another ligand exchange via **TS4** to give a more stable intermediate **Int5**. **TS4** lies 5.5 kcal mol^{-1} below **TS6-(*R*)**, this ligand exchange process is preferred over the spirolactonization process. Intermediate **Int5** then proceeds through a concerted proton transfer/spirolactonization transition state **TS5-(*R*)** to form product and iodoarene with a barrier of 16.6 kcal mol^{-1}. Halogen-bonding interactions also contribute to the stabilization of intermediates and transition states involved in the second spirolactonization process (Figure S4). The ligand-exchange process is the rate-determining step for **K1**-mediated oxidative spirolactonization with an overall activation free energy barrier of 19.8 kcal mol^{-1} (Figure 1b). This is 1.2 kcal mol^{-1} lower than the overall activation free energy barrier of **R1**-mediated oxidative spirolactonization (Figure 1a). Therefore, the second iodine(III) center of **R1** is even slightly more reactive[25] for oxidative spirolactonization, and this process should not be ignored.

On the basis of the above discussion, a revised mechanism is proposed for the spirobiindane-based μ-oxo-bridged hypervalent iodine(III) reagent **R1**-induced asymmetric dearomatizing spirolactonization (Figure 5). In comparison with Kita's mechanism (Figure 1c), the revised mechanism emphasizes (i) the importance of proton transfer from the pendant carboxylic acid of naphthols to the bridging oxygen atom or ligand of iodine(III) species for the dearomatizing spirolactonization; (ii) that halogen-bonding interactions stabilize the dearomatizing spirolactonization transition states, and (iii) that the two iodine(III) centers of the μ-oxo-bridged hypervalent iodine(III) reagent are both capable of transforming naphthol carboxylic acids to spirolactone products. The dearomatizing spirolactonization is the stereocontrolling step for both **R1**- and **K1**-induced asymmetric spirolactonization of naphthol carboxylic acid.

Origin of the Enantioselectivity. With detailed mechanistic information in hand, we next explored the origin of enantioselectivity. The lowest-lying TSs leading to the major and minor enantiomers of products for **R1**- and **K1**-induced dearomatizing spirolactonization are shown in Figure 6. For

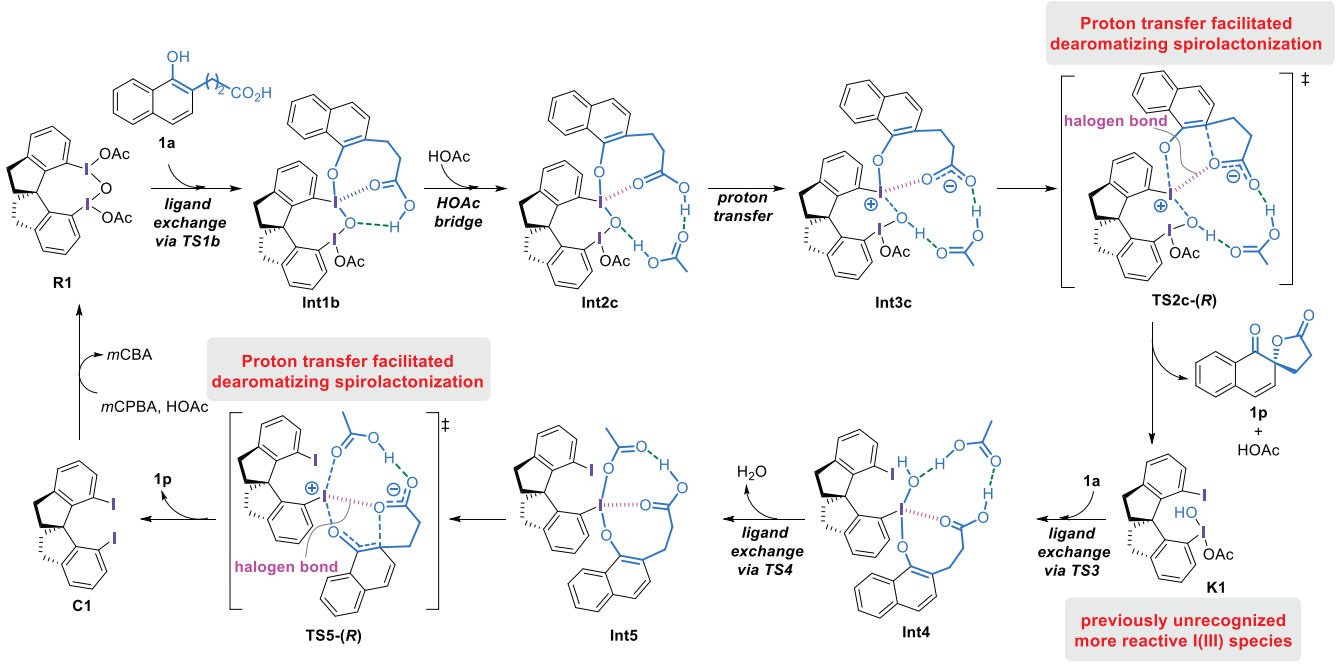

Figure 5. Revised mechanism for the spirobiindane-based μ-oxo-bridged hypervalent iodine(III) reagent **R1**-induced asymmetric dearomatizing spirolactonization.

DOI: 10.1021/jacs.9b08243
J. Am. Chem. Soc. 2019, 141, 16046−16056

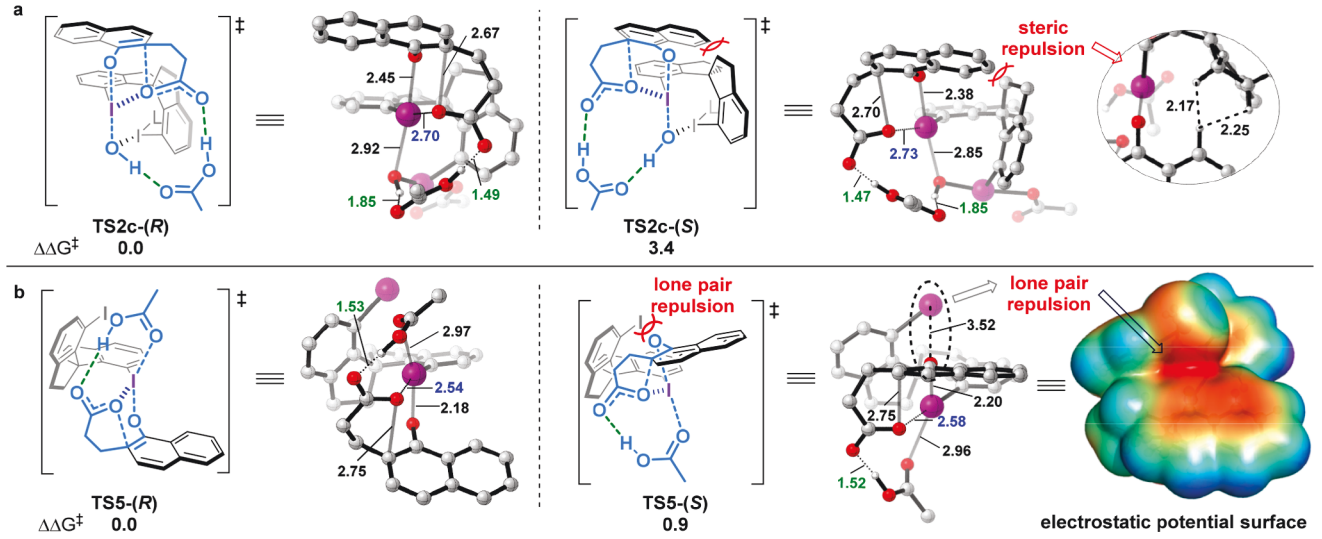

Figure 6. Geometries and relative free energies (kcal mol^{-1}) of enantiomeric TSs for (a) **R1**-induced spirolactonization process and (b) **K1**-induced spirolactonization process. Some hydrogen atoms are not shown for clarity.

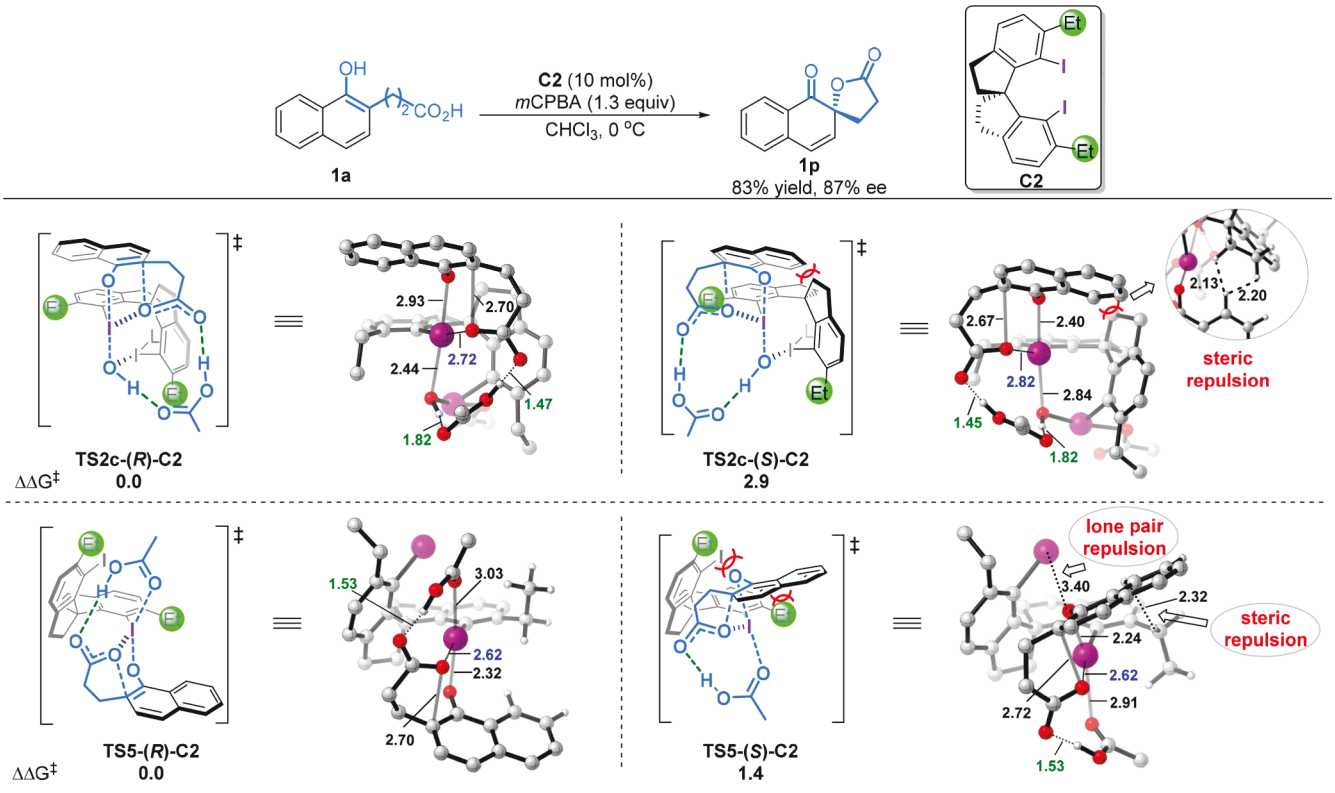

Figure 7. Structures and relative free energies (kcal mol^{-1}) of two pairs of enantiomeric TSs for **C2**-catalyzed asymmetric oxidative Kita spirolactonization of substrate **1a**.

R1-induced spirolactonization, **TS2c-(*R*)**, leading to the experimentally observed major *R* enantiomer of product **1p**, is favored over **TS2c-(*S*)** by 3.4 kcal/mol. In the disfavored **TS2c-(*S*)**, the naphthalene ring points toward the catalyst backbone and suffers steric repulsion (Figure 6a). This destabilizing steric repulsion is avoided in **TS2c-(*R*)** as the naphthalene ring is pointing away from the catalyst backbone. If only this spirolactonization process is considered, the computed $\Delta\Delta G^{\ddagger}$ of 3.4 kcal mol^{-1} yields >99% *ee*, which is greater than that observed experimentally (72% *ee*, ca. 1 kcal mol^{-1}).

For the **K1**-induced spirolactonization process, **TS5-(*S*)** is only 0.9 kcal mol^{-1} higher in free energy than **TS5-(*R*)** (Figure 6b). The difference in free energy appears to come from the lone-pair repulsion between the iodine atom of catalyst and the oxygen atom of naphthol (Figure 6b). This is in line with experimental observation that the spirobiindane compound having one iodine group gave the product **1p** with a poorer *ee* value (19% *ee*).[5c] If only this spirolactonization process is considered, the computed $\Delta\Delta G^{\ddagger}$ of 0.9 kcal mol^{-1} gives 68% *ee*, which is slightly lower than the experimentally observed value of 72% *ee*.

DOI: 10.1021/jacs.9b08243
J. Am. Chem. Soc. 2019, 141, 16046−16056

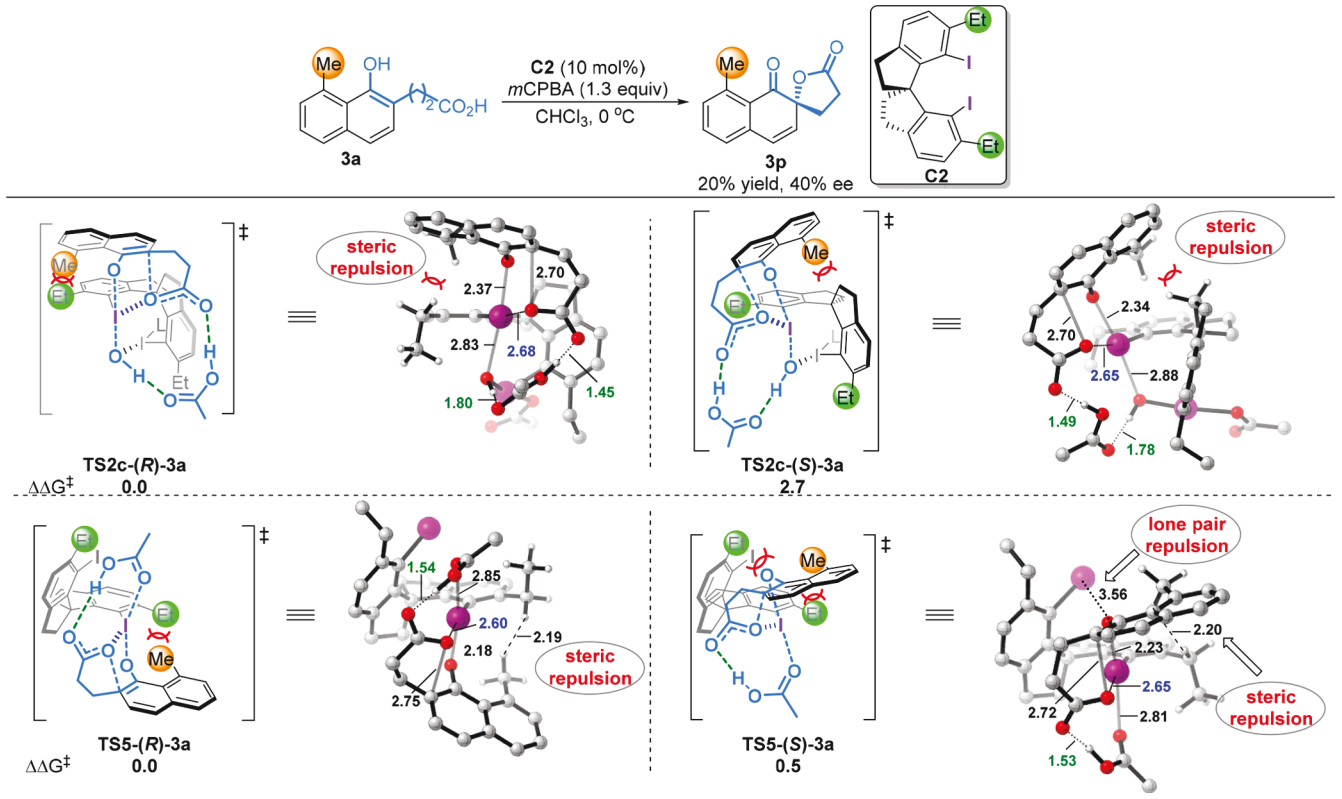

Figure 8. Structures and relative free energies (kcal mol^{-1}) of two pairs of enantiomeric TSs for **C2**-catalyzed asymmetric oxidative Kita spirolactonization of substrate **3a**.

From the above mechanistic discussions, the apparent product enantiomeric excess of this reaction should arise not only from the **R1**-induced spirolactonization process (Figure 1a) but also from the *in situ*-generated **K1**-induced spirolactonization (Figure 1b). Taking both processes into consideration yields 84% *ee* (99% *R* *0.5 + 68% *R* *0.5 = 84% *R*), which is close to the experimentally observed value of 72% *ee*. Clearly, the coexistence of **K1**-mediated spirolactonization in the reaction system, actually, results in a lower apparent selectivity. This gives rise to an interesting question: Why does **R1** induce higher selectivity than **K1**?

Comparison of the two pairs of enantiodetermining TS structures provides insight. Due to the presence of an oxygen bridge in **R1**, the naphthol substrate is restricted to be positioned in the opposite apical position of the iodine(III) in both **TS2c-(*R*)** and **TS2c-(*S*)** (Figure 6a).[5c] The steric repulsion between the naphthalene ring of substrate and catalyst backbone in **TS2c-(*S*)** is unavoidable and strongly destabilizes this structure, thus leading to a high enantioselectivity. In contrast, the oxygen bridge is absent in **K1**. Consequently, in the TS leading to the minor enantiomer, the naphthol substrate could be positioned in the groove of the two spirobiindane planes to avoid the strong steric hindrance caused by the catalyst backbone (see Figure S3). This results in a smaller energy difference (only 0.9 kcal mol^{-1}) between **TS5-(*S*)** and **TS5-(*R*)** (Figure 6b). This is consistent with Kita's observation that the presence of the two iodine groups in the spirobiindane backbone is essential for highly enantioselective control of the catalysts.[5a,c]

Catalyst *ortho*-Substituent Effect on Enantioselectivity. Kita et al. elegantly showed that introducing an ethyl group into the *ortho* position of the iodine atom of the spirobiindane catalyst (**C1**) can improve the selectivity without altering the stereochemistry of the products.[5c] To gain a better understanding of the *ortho*-substituent effect on enantioselectivity, we investigated the stereocontrolling TSs for the *ortho*-ethyl-substituted spirobiindane catalyst **C2**. The results are shown in Figure 7. The computed *ee* value for catalyst **C2** is 93% (99%*0.5 + 86%*0.5 = 93% *R*) in favor of the *R* enantiomer, which is in good agreement with experiment data (87% *R* in $CHCl_3$). The most striking difference in the stereocontrolling TS geometries after *ortho*-ethyl incorporation is the significant shortening of O---I distance in **TS5-(*S*)-C2** (3.40 Å in **TS5-(*S*)-C2**, Figure 7 vs 3.52 Å in **TS5-(*S*)**, Figure 6), forced by the repulsion between the naphthalene ring and the *ortho*-ethyl group. This results in a stronger O---I lone-pair repulsion in **TS5-(*S*)-C2**, leading to a greater $\Delta\Delta G^{\ddagger}$ of 1.4 kcal mol^{-1} (**TS5-(*R*)-C2** vs **TS5-(*S*)-C2**). Consequently, the *ee* increases to 86% for the second spirolactonization process. On the other hand, the *ortho*-substituent hardly influences the enantioselectivity of the first spirolactonization process. The free energy difference between **TS2c-(*R*)-C2** and **TS2c-(*S*)-C2** is still as high as 2.9 kcal mol^{-1}. Therefore, the increased enantioselectivity arises from the second spirolactonization process. More specifically, it is the repulsion between the *ortho*-ethyl group and the naphthalene ring, which causes a stronger O---I lone-pair repulsion in the TS leading to minor enantiomer, that leads to elevated enantioselectivity.

Substrate Substituent Effect on Enantioselectivity. Kita et al. found that introduction of a methyl group at the 8-position of propanoic acid naphthol **1a** resulted in a significant decrease in stereoselectivity (40% *ee*), while substitution at other position maintained good *ee* values.[5c] This observation can be well rationalized by our stereochemical model. Figure 8

DOI: 10.1021/jacs.9b08243
J. Am. Chem. Soc. 2019, 141, 16046−16056

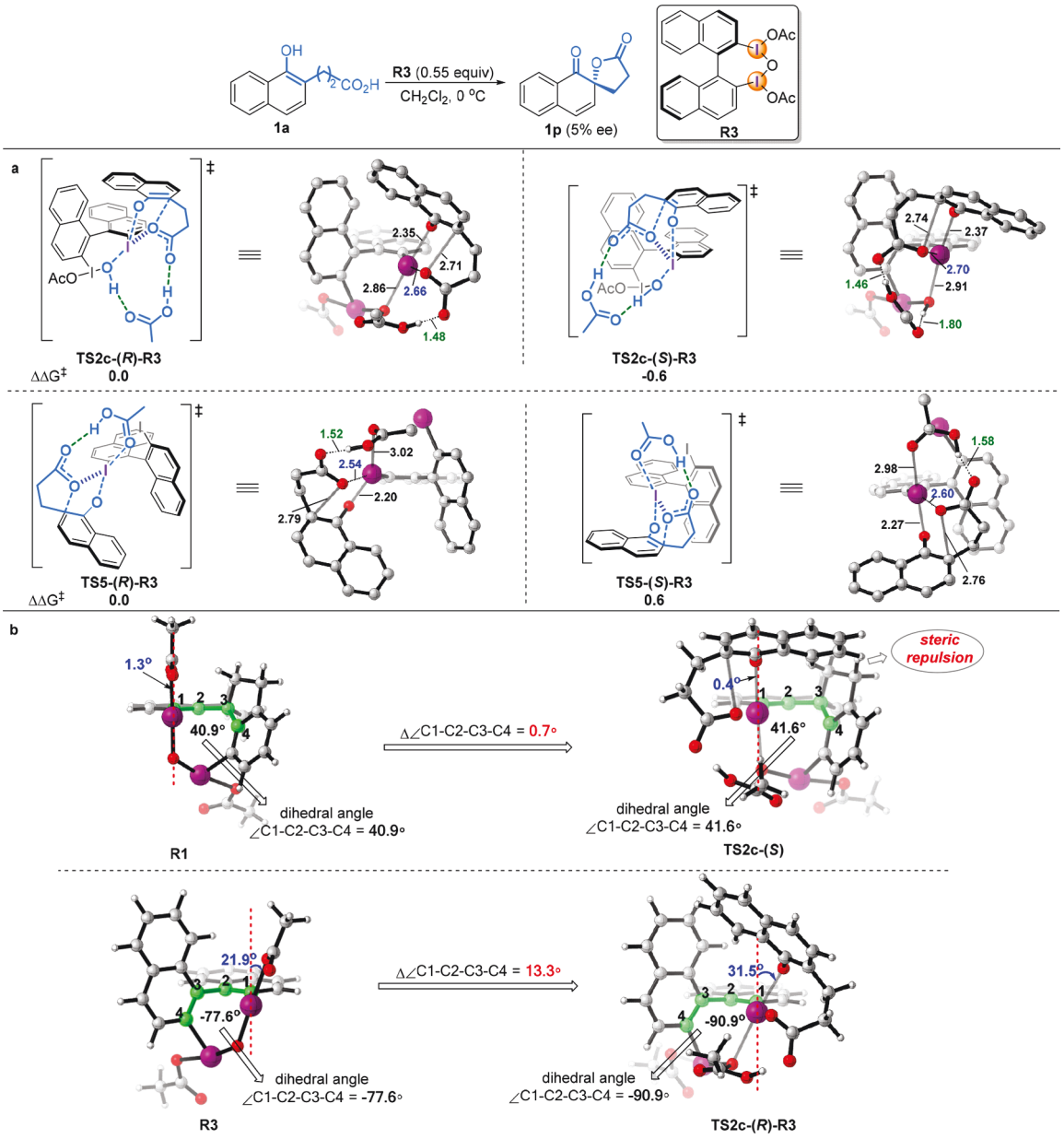

Figure 9. (a) Geometries and relative free energies (kcal mol^{-1}) of enantiomeric TSs for the binaphthyl-based reagent **R3**-mediated asymmetric oxidative Kita spirolactonization. (b) Dihedral angles between two iodoarene planes (∠C1−C2−C3−C4) and degree of deviation of 3-center-4-electron bond from the iodine center (in blue) in **R1**, **R3**, **TS2c-(*S*)**, and **TS2c-(*R*)-R3**.

clearly shows that the introduction of methyl at the 8-position of **1a** gives rise to steric repulsions in the TS leading to the major enantiomers (**TS2c-(*R*)-3a** and **TS5-(*R*)-3a**), thus resulting in a lower selectivity ($\Delta\Delta G^{\ddagger}$ decreases from 2.9 and 1.4 kcal mol^{-1} for substrate **1a** to 2.7 and 0.5 kcal mol^{-1} for substrate **3a**).

Effect of Axially Chiral Scaffold on Enantioselectivity. Axially chiral 1,1′-spirobiindane and 1,1′-binaphthyl both have been classified as "privileged" scaffolds for chiral ligands and catalysts for asymmetric synthesis.[26] Intriguingly, Kita found that the binaphthyl-based hypervalent iodine reagent **R3** gave nearly racemic product (5% ee) for the same reaction (Figure 9).[5a]

To further investigate the effect of axially chiral scaffold on enantioselectivity, we calculated the enantiomeric TS structures and energies for the binaphthyl-based hypervalent iodine reagent **R3**. Consistent with the experimental observations, the difference in free energies between **TS2c-(*R*)-R3** and **TS2c-(*S*)-R3** is only 0.6 kcal mol^{-1} (Figure 9a), which is 2.8 kcal mol^{-1} smaller than the free energy difference between **TS2c-(*R*)** and **TS2c-(*S*)**. As mentioned earlier, the free energy difference between **TS2c-(*R*)** and **TS2c-(*S*)** stems mainly from the steric repulsion between the naphthalene ring and the catalyst's spirobiindane backbone in **TS2c-(*S*)** (Figure 6). When switched from 1,1′-spirobiindane to 1,1′-binaphthyl skeleton, such repulsion is no longer existing in **TS2c-(*R*)-R3**. This is due to the fact that the 1,1′-binaphthyl skeleton is more flexible[27] (with adjustable dihedral angle ∠C1−C2−C3−C4) as compared to the 1,1′-spirobiindane skeleton, which allows it to adjust geometry to avoid the steric repulsion, thus resulting in a considerable loss of selectivity ($\Delta\Delta G^{\ddagger}$ of 0.6 kcal mol^{-1} for **R3** vs $\Delta\Delta G^{\ddagger}$ of 3.4 kcal mol^{-1} for **R1**). Indeed, a noticeable

DOI: 10.1021/jacs.9b08243
J. Am. Chem. Soc. 2019, 141, 16046−16056

change in the dihedral angle between the two iodoarene planes is observed on going from **R3** to **TS2c-(*R*)-R3** (Δ∠C1−C2−C3−C4 = 13.3°, Figure 9b), whereas the dihedral angle remains nearly the same on going from **R1** to **TS2c-(*S*)** (Δ∠C1−C2−C3−C4 = 0.7°).

CONCLUSION

The mechanism and stereoselectivities of asymmetric oxidative dearomatization spirolactonization of naphthol carboxylic acids promoted by the μ-oxo-bridged hypervalent iodine(III) species have been theoretically explored. A revised mechanism and stereocontrol model have been proposed. The revised mechanism emphasizes (i) the importance of proton transfer from the pendant carboxylic acid of naphthols to the bridging oxygen atom or ligand of iodine(III) species for the dearomatizing spirolactonization; (ii) that halogen-bonding interactions stabilize the dearomatizing spirolactonization transition states; and (iii) that the two iodine(III) centers of the μ-oxo-bridged hypervalent iodine(III) reagent are both capable of transforming naphthol carboxylic acids to spirolactone products. The long-neglected second iodine(III) center is more reactive but less selective than the first iodine(III) center. The co-existence of two sequential dearomatizing spirolactonization processes in the reaction system results in a lower apparent enantioselectivity. The new stereochemical model is consistent with the observed experimental results in terms of the selectivity and levels of enantiocontrol as catalyst or substrate variations. It also sheds light on the effects of rigidity and flexibility of catalyst on stereoinduction. Systematic studies of other types of hypervalent iodine(III)-induced asymmetric dearomatizing spirocyclizations are underway in our research group and will be reported in due course.

ASSOCIATED CONTENT

Supporting Information

The Supporting Information is available free of charge on the ACS Publications website at DOI: 10.1021/jacs.9b08243.

Figures S1−S6, and optimized geometries of all species (PDF)

AUTHOR INFORMATION

Corresponding Authors

*houk@chem.ucla.edu

*xuexs@nankai.edu.cn

ORCID

K. N. Houk: 0000-0002-8387-5261

Xiao-Song Xue: 0000-0003-4541-8702

Notes

The authors declare no competing financial interest.

ACKNOWLEDGMENTS

We are grateful for financial support from the Natural Science Foundation of China (Grant Nos. 21772098) and the Fundamental Research Funds for the Central Universities. X.-S.X. appreciates the hospitality provided by Prof. Houk and thanks the Nankai-UCLA Excellent Young Researcher program and National Science Foundation (CHE-1764328 to K.N.H.) for financial support. H.Z. thanks Mr. Taishan Yan for his suggestions and initial work on transition state searching of this study. This paper is dedicated to the 100th anniversaries of both Nankai University and UCLA.

REFERENCES

(1) (a) Yoshimura, A.; Zhdankin, V. V. Advances in Synthetic Applications of Hypervalent Iodine Compounds. *Chem. Rev.* **2016**, *116*, 3328. (b) *Hypervalent Iodine Chemistry*; Wirth, T., Ed.; Springer-Verlag: Berlin, 2016.

(2) For selected reviews, see: (a) Liang, H.; Ciufolini, M. A. Chiral Hypervalent Iodine Reagents in Asymmetric Reactions. *Angew. Chem., Int. Ed.* **2011**, *50*, 11849. (b) Parra, A.; Reboredo, S. Chiral Hypervalent Iodine Reagents: Synthesis and Reactivity. *Chem. - Eur. J.* **2013**, *19*, 17244. (c) Romero, R. M.; Wöste, T. H.; Muñiz, K. Vicinal Difunctionalization of Alkenes with Iodine(III) Reagents and Catalysts. *Chem. - Asian J.* **2014**, *9*, 972. (d) Berthiol, F. Reagent and Catalyst Design for Asymmetric Hypervalent Iodine Oxidations. *Synthesis* **2015**, *47*, 587. (e) Claraz, A.; Masson, G. Asymmetric Iodine Catalysis-Mediated Enantioselective Oxidative Transformations. *Org. Biomol. Chem.* **2018**, *16*, 5386. (f) Cai, Q.; Ma, H. Recent Advances of Chiral Hypervalent Iodine Reagents. *Huaxue Xuebao* **2019**, *77*, 213. (g) Flores, A.; Cots, E.; Berges, J.; Muñiz, K. Enantioselective Iodine(I/III) Catalysis in Organic Synthesis. *Adv. Synth. Catal.* **2019**, *361*, 2.

(3) For selected examples, see: (a) Yu, J.; Cui, J.; Hou, X.-S.; Liu, S.-S.; Gao, W.-C.; Jiang, S.; Tian, J.; Zhang, C. Enantioselective α-Tosyloxylation of Ketones Catalyzed by Spirobiindane Scaffold-Based Chiral Iodoarenes. *Tetrahedron: Asymmetry* **2011**, *22*, 2039. (b) Suzuki, S.; Kamo, T.; Fukushi, K.; Hiramatsu, T.; Tokunaga, E.; Dohi, T.; Kita, Y.; Shibata, N. Iodoarene-Catalyzed Fluorination and Aminofluorination by An Ar-I/HF·pyridine/*m*CPBA System. *Chem. Sci.* **2014**, *5*, 2754. (c) Wu, H.; He, Y.-P.; Xu, L.; Zhang, D.-Y.; Gong, L.-Z. Asymmetric Organocatalytic Direct C(sp^2)-H/C(sp^3)-H Oxidative Cross-Coupling by Chiral Iodine Reagents. *Angew. Chem., Int. Ed.* **2014**, *53*, 3466. (d) Basdevant, B.; Legault, C. Y. Enantioselective Iodine(III)-Mediated Synthesis of α-Tosyloxy Ketones: Breaking the Selectivity Barrier. *Org. Lett.* **2015**, *17*, 4918. (e) Levitre, G.; Dumoulin, A.; Retailleau, P.; Panossian, A.; Leroux, F. R.; Masson, G. Asymmetric α-Sulfonyl- and α-Phosphoryl-Oxylation of Ketones by a Chiral Hypervalent Iodine(III). *J. Org. Chem.* **2017**, *82*, 11877. (f) Wang, Y.; Yuan, H.; Lu, H.; Zheng, W. H. Development of Planar Chiral Iodoarenes Based on [2.2]-Paracyclophane and Their Application in Catalytic Enantioselective Fluorination of beta-Ketoesters. *Org. Lett.* **2018**, *20*, 2555. (g) Zhang, D.-Y.; Zhang, Y.; Wu, H.; Gong, L.-Z. Organoiodine-Catalyzed Enantioselective Alkoxylation/Oxidative Rearrangement of Allylic Alcohols. *Angew. Chem., Int. Ed.* **2019**, *58*, 7450.

(4) For selected examples, see: (a) Fujita, M.; Yoshida, Y.; Miyata, K.; Wakisaka, A.; Sugimura, T. Enantiodifferentiating *endo*-Selective Oxylactonization of *ortho*-Alk-1-enylbenzoate with a Lactate-Derived Aryl-λ^3-Iodane. *Angew. Chem., Int. Ed.* **2010**, *49*, 7068. (b) Kong, W.; Feige, P.; de Haro, T.; Nevado, C. Regio- and Enantioselective Aminofluorination of Alkenes. *Angew. Chem., Int. Ed.* **2013**, *52*, 2469. (c) Banik, S. M.; Medley, J. W.; Jacobsen, E. N. Catalytic, Asymmetric Difluorination of Alkenes to Generate Difluoromethylated Stereocenters. *Science* **2016**, *353*, 51. (d) Haubenreisser, S.; Wöste, T. H.; Martínez, C.; Ishihara, K.; Muñiz, K. Structurally Defined Molecular Hypervalent Iodine Catalysts for Intermolecular Enantioselective Reactions. *Angew. Chem., Int. Ed.* **2016**, *55*, 413. (e) Shimogaki, M.; Fujita, M.; Sugimura, T. Metal-Free Enantioselective Oxidative Arylation of Alkenes: Hypervalent-Iodine-Promoted Oxidative C−C Bond Formation. *Angew. Chem., Int. Ed.* **2016**, *55*, 15797. (f) Woerly, E. M.; Banik, S. M.; Jacobsen, E. N. Enantioselective, Catalytic Fluorolactonization Reactions with a Nucleophilic Fluoride Source. *J. Am. Chem. Soc.* **2016**, *138*, 13858. (g) Muñiz, K.; Barreiro, L.; Romero, R. M.; Martínez, C. Catalytic Asymmetric Diamination of Styrenes. *J. Am. Chem. Soc.* **2017**, *139*, 4354. (h) Mennie, K. M.; Banik, S. M.; Reichert, E. C.; Jacobsen, E. N. Catalytic Diastereo- and Enantioselective Fluoroamination of Alkenes. *J. Am. Chem. Soc.* **2018**, *140*, 4797.

DOI: 10.1021/jacs.9b08243
J. Am. Chem. Soc. 2019, 141, 16046−16056

(5) For selected examples, see: (a) Dohi, T.; Maruyama, A.; Takenaga, N.; Senami, K.; Minamitsuji, Y.; Fujioka, H.; Caemmerer, S. B.; Kita, Y. A Chiral Hypervalent Iodine(III) Reagent for Enantioselective Dearomatization of Phenols. *Angew. Chem., Int. Ed.* **2008**, *47*, 3787. (b) Uyanik, M.; Yasui, T.; Ishihara, K. Enantioselective Kita Oxidative Spirolactonization Catalyzed by In Situ Generated Chiral Hypervalent Iodine(III) Species. *Angew. Chem., Int. Ed.* **2010**, *49*, 2175. (c) Dohi, T.; Takenaga, N.; Nakae, T.; Toyoda, Y.; Yamasaki, M.; Shiro, M.; Fujioka, H.; Maruyama, A.; Kita, Y. Asymmetric Dearomatizing Spirolactonization of Naphthols Catalyzed by Spirobiindane-Based Chiral Hypervalent Iodine Species. *J. Am. Chem. Soc.* **2013**, *135*, 4558. (d) Uyanik, M.; Yasui, T.; Ishihara, K. Hydrogen Bonding and Alcohol Effects in Asymmetric Hypervalent Iodine Catalysis: Enantioselective Oxidative Dearomatization of Phenols. *Angew. Chem., Int. Ed.* **2013**, *52*, 9215. (e) Uyanik, M.; Sasakura, N.; Mizuno, M.; Ishihara, K. Enantioselective Synthesis of Masked Benzoquinones Using Designer Chiral Hypervalent Organoiodine(III) Catalysis. *ACS Catal.* **2017**, *7*, 872. (f) Dohi, T.; Sasa, H.; Miyazaki, K.; Fujitake, M.; Takenaga, N.; Kita, Y. Chiral Atropisomeric 8,8′-Diiodobinaphthalene for Asymmetric Dearomatizing Spirolactonizations in Hypervalent Iodine Oxidations. *J. Org. Chem.* **2017**, *82*, 11954. (g) Ogasawara, M.; Sasa, H.; Hu, H.; Amano, Y.; Nakajima, H.; Takenaga, N.; Nakajima, K.; Kita, Y.; Takahashi, T.; Dohi, T. Atropisomeric Chiral Diiododienes (Z,Z)-2,3-Di(1-iodoalkylidene)tetralins: Synthesis, Enantiomeric Resolution, and Application in Asymmetric Catalysis. *Org. Lett.* **2017**, *19*, 4102. (h) Hashimoto, T.; Shimazaki, Y.; Omatsu, Y.; Maruoka, K. Indanol-Based Chiral Organoiodine Catalysts for Enantioselective Hydrative Dearomatization. *Angew. Chem., Int. Ed.* **2018**, *57*, 7200. (i) Ding, Q.; He, H.; Cai, Q. Chiral Aryliodine-Catalyzed Asymmetric Oxidative C-N Bond Formation via Desymmetrization Strategy. *Org. Lett.* **2018**, *20*, 4554.

(6) (a) Sreenithya, A.; Patel, C.; Hadad, C. M.; Sunoj, R. B. Hypercoordinate Iodine Catalysts in Enantioselective Transformation: The Role of Catalyst Folding in Stereoselectivity. *ACS Catal.* **2017**, *7*, 4189. (b) Pluta, R.; Krach, P. E.; Cavallo, L.; Falivene, L.; Rueping, M. Metal-Free Catalytic Asymmetric Fluorination of Keto Esters Using a Combination of Hydrogen Fluoride (HF) and Oxidant: Experiment and Computation. *ACS Catal.* **2018**, *8*, 2582. (c) Zhou, B.; Haj, M. K.; Jacobsen, E. N.; Houk, K. N.; Xue, X.-S. Mechanism and Origins of Chemo- and Stereoselectivities of Aryl Iodide-Catalyzed Asymmetric Difluorinations of β-Substituted Styrenes. *J. Am. Chem. Soc.* **2018**, *140*, 15206. (d) Sreenithya, A.; Hadad, C. M.; Sunoj, R. B. Hypercoordinate Iodine for Catalytic Asymmetric Diamination of Styrene: Insights into the Mechanism, Role of Solvent, and Stereoinduction. *Chem. Sci.* **2019**, *10*, 7082.

(7) For reviews, see: (a) Harned, A. M. Asymmetric Oxidative Dearomatizations Promoted by Hypervalent Iodine(III) Reagents: an Opportunity for Rational Catalyst Design? *Tetrahedron Lett.* **2014**, *55*, 4681. (b) Fujita, M. Mechanistic Aspects of Alkene Oxidation Using Chiral Hypervalent Iodine Reagents. *Tetrahedron Lett.* **2017**, *58*, 4409. (c) Sreenithya, A.; Surya, K.; Sunoj, R. B. Hypercoordinate Iodine(III) Promoted Reactions and Catalysis: An Update on Current Mechanistic Understanding. *Wires Comput. Mol. Sci.* **2017**, *7*, e1299. For selected examples, see: (d) Sreenithya, A.; Sunoj, R. B. Mechanistic Insights on Iodine(III) Promoted Metal-Free Dual C-H Activation Involved in the Formation of a Spirocyclic Bis-oxindole. *Org. Lett.* **2014**, *16*, 6224. (e) Beaulieu, S.; Legault, C. Y. Mechanistic Insights on the Iodine(III)-Mediated α-Oxidation of Ketones. *Chem. - Eur. J.* **2015**, *21*, 11206. (f) Funes-Ardoiz, I.; Sameera, W. M. C.; Romero, R. M.; Martínez, C.; Souto, J. A.; Sampedro, D.; Muñiz, K.; Maseras, F. DFT Rationalization of the Diverse Outcomes of the Iodine(III)-Mediated Oxidative Amination of Alkenes. *Chem. - Eur. J.* **2016**, *22*, 7545. (g) Liu, L.; Zhang, T.; Yang, Y.-F.; Zhang-Negrerie, D.; Zhang, X.; Du, Y.; Wu, Y.-D.; Zhao, K. Metal-Free Synthesis of 3-Arylquinolin-2-ones from Acrylic Amides via a Highly Regioselective 1,2-Aryl Migration: An Experimental and Computational Study. *J. Org. Chem.* **2016**, *81*, 4058. (h) Harned, A. M. Concerning the Mechanism of Iodine(III)-Mediated Oxidative Dearomatization of Phenols. *Org. Biomol. Chem.* **2018**, *16*, 2324. (i) Tang, T.; Harned, A. M. Experimental Evidence for the Formation of Cationic Intermediates During Iodine(III)-Mediated Oxidative Dearomatization of Phenols. *Org. Biomol. Chem.* **2018**, *16*, 8249. (j) Ganji, B.; Ariafard, A. DFT Mechanistic Investigation into Phenol Dearomatization Mediated by an Iodine(III) Reagent. *Org. Biomol. Chem.* **2019**, *17*, 3521. (k) Shu, S.; Li, Y.; Jiang, J.; Ke, Z.; Liu, Y. Mechanism of Hypervalent Iodine Promoted Fluorocyclization of Unsaturated Alcohols: Metathesis via Double Acids Activation. *J. Org. Chem.* **2019**, *84*, 458.

(8) (a) Pouységu, L.; Deffieux, D.; Quideau, S. Hypervalent Iodine-Mediated Phenol Dearomatization in Natural Product Synthesis. *Tetrahedron* **2010**, *66*, 2235. (b) Roche, S. P.; Porco, J. A., Jr. Dearomatization Strategies in the Synthesis of Complex Natural Products. *Angew. Chem., Int. Ed.* **2011**, *50*, 4068. (c) Zhuo, C.-X.; Zhang, W.; You, S.-L. Catalytic Asymmetric Dearomatization Reactions. *Angew. Chem., Int. Ed.* **2012**, *51*, 12662. (d) Sun, W.; Li, G.; Hong, L.; Wang, R. Asymmetric Dearomatization of Phenols. *Org. Biomol. Chem.* **2016**, *14*, 2164. (e) Wu, W.-T.; Zhang, L.; You, S.-L. Catalytic Asymmetric Dearomatization (CADA) Reactions of Phenol and Aniline Derivatives. *Chem. Soc. Rev.* **2016**, *45*, 1570. (f) *Asymmetric Dearomatization Reactions*; You, S.-L., Ed.; Wiley-VCH: Weinheim, Germany, 2016.

(9) (a) Kwon, Y.; Li, J.; Reid, J. P.; Crawford, J. M.; Jacob, R.; Sigman, M. S.; Toste, F. D.; Miller, S. J. Disparate Catalytic Scaffolds for Atroposelective Cyclodehydration. *J. Am. Chem. Soc.* **2019**, *141*, 6698. (b) Crawford, J. M.; Sigman, M. S. Conformational Dynamics in Asymmetric Catalysis: Is Catalyst Flexibility a Design Element? *Synthesis* **2019**, *51*, 1021.

(10) Frisch, M. J.; Trucks, G. W.; Schlegel, H. B.; Scuseria, G. E.; Robb, M. A.; Cheeseman, J. R.; Scalmani, G.; Barone, V.; Mennucci, B.; Petersson, G. A.; Nakatsuji, H.; Caricato, M.; Li, X.; Hratchian, H. P.; Izmaylov, A. F.; Bloino, J.; Zheng, G.; Sonnenberg, J. L.; Hada, M.; Ehara, M.; Toyota, K.; Fukuda, R.; Hasegawa, J.; Ishida, M.; Nakajima, T.; Honda, Y.; Kitao, O.; Nakai, H.; Vreven, T.; Montgomery, J. A., Jr.; Peralta, J. E.; Ogliaro, F.; Bearpark, M.; Heyd, J. J.; Brothers, E.; Kudin, K. N.; Staroverov, V. N.; Kobayashi, R.; Normand, J.; Raghavachari, K.; Rendell, A.; Burant, J. C.; Iyengar, S. S.; Tomasi, J.; Cossi, M.; Rega, N.; Millam, J. M.; Klene, M.; Knox, J. E.; Cross, J. B.; Bakken, V.; Adamo, C.; Jaramillo, J.; Gomperts, R.; Stratmann, R. E.; Yazyev, O.; Austin, A. J.; Cammi, R.; Pomelli, C.; Ochterski, J. W.; Martin, R. L.; Morokuma, K.; Zakrzewski, V. G.; Voth, G. A.; Salvador, P.; Dannenberg, J. J.; Dapprich, S.; Daniels, A. D.; Farkas, O.; Foresman, J. B.; Ortiz, J. V.; Cioslowski, J.; Fox, D. J. *Gaussian 09*, revision D.01; Gaussian, Inc., Wallingford, CT, 2013.

(11) Zhao, Y.; Truhlar, D. G. Density Functionals with Broad Applicability in Chemistry. *Acc. Chem. Res.* **2008**, *41*, 157.

(12) Andrae, D.; Häußermann, U.; Dolg, M.; Stoll, H.; Preuß, H. Energy-Adjusted *ab initio* Pseudopotentials for the Second and Third Row Transition Elements. *Theor. Chim. Acta* **1990**, *77*, 123.

(13) (a) Marenich, A. V.; Cramer, C. J.; Truhlar, D. G. Universal Solvation Model Based on Solute Electron Density and on a Continuum Model of the Solvent Defined by the Bulk Dielectric Constant and Atomic Surface Tensions. *J. Phys. Chem. B* **2009**, *113*, 6378. (b) Engelage, E.; Schulz, N.; Heinen, F.; Huber, S. M.; Truhlar, D. G.; Cramer, C. J. Refined SMD Parameters for Bromine and Iodine Accurately Model Halogen-Bonding Interactions in Solution. *Chem. - Eur. J.* **2018**, *24*, 15983.

(14) (a) Frei, R.; Wodrich, M. D.; Hari, D. P.; Borin, P.-A.; Chauvier, C.; Waser, J. Fast and Highly Chemoselective Alkynylation of Thiols with Hypervalent Iodine Reagents Enabled through a Low Energy Barrier Concerted Mechanism. *J. Am. Chem. Soc.* **2014**, *136*, 16563. (b) Zhu, C.; Liang, Y.; Hong, X.; Sun, H.; Sun, W.-Y.; Houk, K. N.; Shi, Z. Iodoarene-Catalyzed Stereospecific Intramolecular sp^3 C−H Amination: Reaction Development and Mechanistic Insights. *J. Am. Chem. Soc.* **2015**, *137*, 7564. (c) Sun, T.-Y.; Wang, X.; Geng, H.; Xie, Y.; Wu, Y.-D.; Zhang, X.; Schaefer, H. F. Why Does Togni's Reagent I Exist in the High-Energy Hypervalent Iodine Form? Re-Evaluation of Benziodoxole Based Hypervalent Iodine Reagents.

DOI: 10.1021/jacs.9b08243
J. Am. Chem. Soc. 2019, 141, 16046−16056

Chem. Commun. **2016**, *52*, 5371. (d) Jiang, H.; Sun, T.-Y.; Wang, X.; Xie, Y.; Zhang, X.; Wu, Y.-D.; Schaefer, H. F. A Twist of the Twist Mechanism, 2-Iodoxybenzoic Acid (IBX)-Mediated Oxidation of Alcohol Revisited: Theory and Experiment. *Org. Lett.* **2017**, *19*, 6502. (e) Yang, J.-D.; Li, M.; Xue, X.-S. Computational I(III)—X BDEs for Benziodoxol(on)e-based Hypervalent Iodine Reagents: Implications for Their Functional Group Transfer Abilities. *Chin. J. Chem.* **2019**, *37*, 359−363.

(15) Peterson, K. A.; Woon, D. E.; Dunning, T. H. Benchmark Calculations with Correlated Molecular Wave Functions. IV. The Classical Barrier Height of the $H+H_2 \rightarrow H_2+H$ Reaction. *J. Chem. Phys.* **1994**, *100*, 7410.

(16) (a) Ayala, P. Y.; Schlegel, H. B. Identification and Treatment of Internal Rotation in Normal Mode Vibrational Analysis. *J. Chem. Phys.* **1998**, *108*, 2314. (b) Ribeiro, R. F.; Marenich, A. V.; Cramer, C. J.; Truhlar, D. G. Use of Solution-Phase Vibrational Frequencies in Continuum Models for the Free Energy of Solvation. *J. Phys. Chem. B* **2011**, *115*, 14556.

(17) Johnson, E. R.; Keinan, S.; Mori-Sánchez, P.; Contreras-García, J.; Cohen, A. J.; Yang, W. Revealing Noncovalent Interactions. *J. Am. Chem. Soc.* **2010**, *132*, 6498.

(18) Legault, C. Y. *CYLview*, 1.0b; Universite de Sherbrooke: Quebec, Canada, 2009; http://www.cylview.org.

(19) *The PyMOL Molecular Graphics System*, Version 2.0.4, Schrödinger, LLC.

(20) Maji, R.; Wheeler, S. E. Importance of Electrostatic Effects in the Stereoselectivity of NHC-Catalyzed Kinetic Resolutions. *J. Am. Chem. Soc.* **2017**, *139*, 12441.

(21) (a) Xia, Y.; Liang, Y.; Chen, Y.; Wang, M.; Jiao, L.; Huang, F.; Liu, S.; Li, Y.; Yu, Z.-X. An Unexpected Role of a Trace Amount of Water in Catalyzing Proton Transfer in Phosphine-Catalyzed (3 + 2) Cycloaddition of Allenoates and Alkenes. *J. Am. Chem. Soc.* **2007**, *129*, 3470. (b) Wang, Y.; Yu, Z.-X. Sigmatropic Proton Shifts: A Quantum Chemical Study. *Org. Biomol. Chem.* **2017**, *15*, 7439. (c) Wang, Y.; Cai, P.-J.; Yu, Z.-X. Carbanion Translocations via Intramolecular Proton Transfers: A Quantum Chemical Study. *J. Org. Chem.* **2017**, *82*, 4604. (d) Wang, Y.; Yu, Z.-X. Intra- versus Intermolecular Carbon-to-Carbon Proton Transfers in the Reactions of Arynes with Nitrogen Nucleophiles: A DFT Study. *J. Org. Chem.* **2018**, *83*, 5384.

(22) (a) Pinto de Magalhães, H.; Togni, A.; Lüthi, H. P. Importance of Nonclassical σ-Hole Interactions for the Reactivity of λ^3-Iodane Complexes. *J. Org. Chem.* **2017**, *82*, 11799. (b) Heinen, F.; Engelage, E.; Dreger, A.; Weiss, R.; Huber, S. M. Iodine(III) Derivatives as Halogen Bonding Organocatalysts. *Angew. Chem., Int. Ed.* **2018**, *57*, 3830.

(23) (a) Bulfield, D.; Huber, S. M. Halogen Bonding in Organic Synthesis and Organocatalysis. *Chem. - Eur. J.* **2016**, *22*, 14434. (b) Cavallo, G.; Metrangolo, P.; Milani, R.; Pilati, T.; Priimagi, A.; Resnati, G.; Terraneo, G. The Halogen Bond. *Chem. Rev.* **2016**, *116*, 2478. (c) Vogel, L.; Wonner, P.; Huber, S. M. Chalcogen Bonding: An Overview. *Angew. Chem., Int. Ed.* **2019**, *58*, 1880.

(24) (a) Ochiai, M.; Sueda, T.; Miyamoto, K.; Kiprof, P.; Zhdankin, V. V. *trans* Influences on Hypervalent Bonding of Aryl λ^3-Iodanes: Their Stabilities and Isodesmic Reactions of Benziodoxolones and Benziodazolones. *Angew. Chem., Int. Ed.* **2006**, *45*, 8203. (b) Sajith, P. K.; Suresh, C. H. Quantification of the Trans Influence in Hypervalent Iodine Complexes. *Inorg. Chem.* **2012**, *51*, 967. (c) Jiang, H.; Sun, T.-Y.; Chen, Y.; Zhang, X.; Wu, Y.-D.; Xie, Y.; Schaefer, H. F. Designing New Togni Reagents by Computation. *Chem. Commun.* **2019**, *55*, 5667.

(25) Previous experimental studies have reported that the cleaved μ-oxo species showed higher reactivities in several oxidations. For examples, see: (a) Gallos, J.; Varvoglis, A.; Alcock, N. W. Oxo-Bridged Compounds of Iodine(III): Syntheses, Structure, and Properties of μ-Oxo-bis[trifluoroacetato(phenyl)iodine]. *J. Chem. Soc., Perkin Trans. 1* **1985**, 757. (b) Takenaga, N.; Uchiyama, T.; Kato, D.; Fujioka, H.; Dohi, T.; Kita, Y. Efficient Phenolic Oxidations to Construct *ortho*-Spirolactone Structures Using Oxo-Bridged Hypervalent Iodine(III) Compound. *Heterocycles* **2010**, *82*, 1327. (c) Dohi, T.; Uchiyama, T.; Yamashita, D.; Washimi, N.; Kita, Y. Efficient Phenolic Oxidations Using μ-Oxo-Bridged Phenyliodine Trifluoroacetate. *Tetrahedron Lett.* **2011**, *52*, 2212.

(26) *Privileged Chiral Ligands and Catalysts*; Zhou, Q.-L., Ed.; Wiley-VCH: Weinheim, Germany, 2011.

(27) As suggested by one reviewer, we computed the enantiomeric transition states for 8,8′-diiodobinaphthalene (**C4**) and 2,2′-dimethyl-8,8′-diiodo-1,1′-binaphthalene (**C5**), a new type of binaphthyl-based chiral iodide catalyst recently developed by Kita and co-workers (see ref 5f), which catalyzed asymmetric oxidative spirolactonization of substrate **1a**. Our computations reproduce well the improved enantioselectivities for the new type of binaphthyl-based chiral iodide catalyst. Indeed, the 8,8′-diiodobinaphthalene catalyst **C4** is more rigid than the 2,2′-diiodobinaphthalene-based reagent **R3**, explaining why increased enantioselectivities could be obtained. For detailed discussion, see Figures S5 and S6.

DOI: 10.1021/jacs.9b08243
J. Am. Chem. Soc. 2019, 141, 16046−16056